Coherent perfect absorber and laser modes in purely imaginary metamaterials

Yangyang Fu,[1,2] Yanyan Cao,[1] Steven A. Cummer,[3] Yadong Xu,[1,*] and Huanyang Chen[1,2,†]
[1]*College of Physics, Optoelectronics and Energy, Soochow University, Suzhou 215006, China*
[2]*Institute of Electromagnetics and Acoustics and Department of Electronic Science, Xiamen University, Xiamen 361005, China*
[3]*Department of Electrical and Computer Engineering, Duke University, Durham, North Carolina 27708, USA*
(Received 24 January 2017; published 16 October 2017)

Conjugate metamaterials, in which the permittivity and the permeability are complex conjugates of each other, possess the elements of loss and gain simultaneously. By employing a conjugate metamaterial with a purely imaginary form, we propose a mechanism for realizing both coherent perfect absorber (CPA) and laser modes. Moreover, the general conditions for obtaining CPA and laser modes, including obtaining them simultaneously, are revealed by analyzing the wave scattering properties of a slab made of purely imaginary metamaterials (PIMs). Specifically, in a PIM slab with a subunity effective refractive index, the CPA mode can be simplified as a perfect absorption mode and the incident wave from one side could be perfectly absorbed.

DOI: 10.1103/PhysRevA.96.043838

I. INTRODUCTION

Metamaterials [1,2] provide unprecedented approaches to manipulate electromagnetic (EM) wave propagation. With them, a number of amazing optical phenomena and devices have been proposed and demonstrated well in experiments, such as the invisibility cloak [3,4], the perfect lens [5,6], field rotators [7,8], and illusion optics [9,10]. All these cases rely on control of the real parts of both the permittivity and permeability of metamaterials. On the other hand, the imaginary parts (i.e., the material gain or loss) also exhibit significant impact on the propagation behavior and characteristics of EM waves. For example, by constructing balanced loss and gain in materials to meet the parity-time (PT) symmetry condition, i.e., $n(x) = n(-x)^*$, many significant propagation effects of light have been revealed, such as unidirectional invisibility [11,12], coherent perfect absorption [13–15], lasing [16,17], and extraordinary nonlinear effects [18,19]. Furthermore, by introducing the gain or loss acting as new freedoms to classify all possible metamaterials, the conventional two-dimensional plane could be expanded to three-dimensional space [20]. Such operation greatly enriches the types of metamaterials, and most of their EM properties are unclear, deserving further investigation.

One group of interest is the so-called conjugate metamaterials (CMs) [20] whose relative permittivity and permeability are complex conjugates of each other in their phases, i.e., $\varepsilon' = \varepsilon e^{-i\alpha}$ and $\mu' = \mu e^{i\alpha}$, where ε and μ are positive numbers and α is the phase factor of the materials. Although they possess the elements of loss and gain simultaneously, their refractive indices are strictly real, and in such media unattenuated propagation of EM waves can be obtained [21,22]. Moreover, the EM properties of CMs are largely dependent of the phase factor α. It has been demonstrated in Ref. [20] that for $0 \leqslant \alpha < \pi/2$, CMs have a positive refractive index, while for $\pi/2 < \alpha \leqslant \pi$, CMs have a negative one. Such CMs might be used to serve as subwavelength-resolution lens with a perfect lens as the limiting case [20]. In particular, when $\alpha = \pi/2$, we define the corresponding CMs as purely imaginary metamaterials (PIMs), which are given by $\varepsilon' = -i\varepsilon$ and $\mu' = i\mu$. As the transition case [20] from positive to negative refractive index, PIMs offer interesting underlying physics to explore.

In this work, for simplicity, $\varepsilon = \mu$ is set for PIMs to uncover significant new behavior of waves (similar wave propagation will still happen for PIMs with $\varepsilon \neq \mu$). We thoroughly study the EM wave behavior in PIMs and find that both coherent perfect absorber (CPA) and laser modes can be supported in a slab composed of PIMs. By analyzing the wave scattering properties of a PIM slab, we deduce the general conditions for realizing CPA and laser modes, which are verified by numerical simulations. We also derive the conditions for obtaining CPA and laser modes simultaneously. Furthermore, when the PIMs are provided with a subunity effective refractive index, there is critical angle for wave impinging from air to them. In contrast to the traditional case, where total reflection happens for the incident angle beyond the critical angle, a PIM slab can function as a perfect absorber (i.e., a simplified CPA mode), absorbing the single-sided incident wave without any reflection and transmission.

II. WAVE SCATTERING OF A PIM SLAB

We first investigate wave scattering from a PIM slab in air, which is schematically shown in Fig. 1(a). The blue dashed and red solid arrows are the incoming and outgoing waves in air, respectively, and the black arrows are the forward and backward waves inside the slab. The EM parameters of PIMs are given as $\varepsilon' = -i\varepsilon$ and $\mu' = i\mu$ for the transverse electric (TE) polarization (the electric field is in the z direction). In this work we will focus on the case of TE polarization. Similar results can be obtained for the transverse magnetic (TM) polarization (the magnetic field is in the z direction). Here the related parameters ε and μ are real numbers; as a result, the effective refractive index of PIMs is $n' = \sqrt{\varepsilon'\mu'} = \sqrt{\varepsilon\mu}$, which is a real number.

The EM parameters of PIMs contain gain and loss simultaneously. Therefore, depending on which dominates in our PIM slab, an incident wave might induce quite intense transmission and reflection defined as laser modes, and as a

*ydxu@suda.edu.cn
†kenyon@xmu.edu.cn

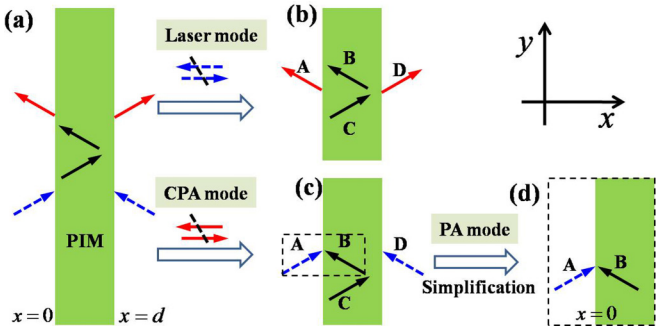

FIG. 1. (a) General schematic diagram of wave scattering for the PIM slab in air. Also shown are the corresponding schematic diagrams of wave scattering for (b) laser modes and (c) CPA modes. (d) Schematic diagram of wave scattering for PA modes in semi-infinite spaces consisting of air and a PIM medium, which are treated as the simplified cases of CPA modes.

result the injected signal (blue dashed arrows) can be ignored [see the schematic diagram in Fig. 1(b)]. Alternatively, if the loss dominates, the slab may support CPA modes, which might absorb incoming coherent waves without any outgoing waves (or reflections). The schematic diagram for obtaining the CPA mode is displayed in Fig. 1(c).

By analyzing the wave scattering of laser modes and CPA modes (for details, see Appendix A), the dispersion relationships of laser modes are expressed as

$$\eta = -i\cot\left(k_x'\frac{d}{2}\right) \quad \text{(odd modes)}, \tag{1}$$

$$\eta = i\tan\left(k_x'\frac{d}{2}\right) \quad \text{(even modes)} \tag{2}$$

and the corresponding dispersion relationships of CPA modes are written as

$$\eta = i\cot\left(k_x'\frac{d}{2}\right) \quad \text{(odd modes)}, \tag{3}$$

$$\eta = -i\tan\left(k_x'\frac{d}{2}\right) \quad \text{(even modes)}, \tag{4}$$

where $\eta = k_x\mu'/k_x'$, $k_x = \sqrt{k_0^2 - \beta^2}$, $k_x' = \sqrt{n'^2k_0^2 - \beta^2}$, $n'^2 = \varepsilon'\mu' = \varepsilon\mu$, β is the propagation constant in the y direction, and k_x and k_x' are the wave vectors in the x direction in air and PIMs, respectively. Even modes are defined as symmetric modes, i.e., the field distribution in the x direction is symmetric, and odd modes are antisymmetric modes, i.e., the field distribution in the x direction is antisymmetric. In fact, for a single slab composed of PIMs ($\varepsilon = \mu$ or $\varepsilon \neq \mu$), the above dispersion relationships are satisfied. Accordingly, CPA and laser modes can be perfectly excited owing to the real solutions for β in Eqs. (1)–(4), while for CMs with $\alpha \neq \pi/2$, i.e., CMs with real parts, there are complex solutions for β. As a result, perfect excitation for CPA and laser modes will not happen and the performance of CPA and laser modes will decrease (for a more detailed discussion, see Appendix A).

Furthermore, under some circumstances (we will explain in Sec. II B), the problem of two coherent incoming waves

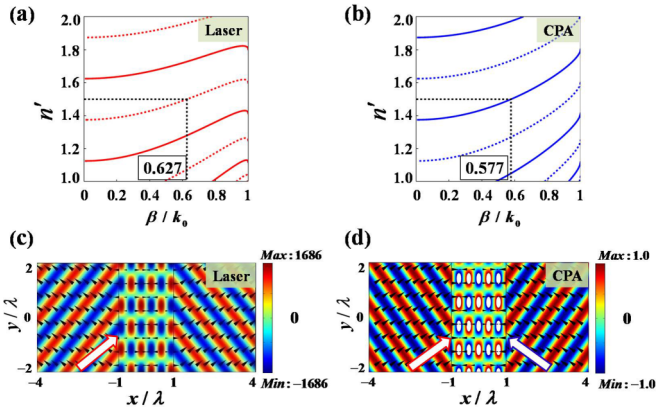

FIG. 2. Corresponding dispersion relationships (n' vs β) for (a) laser modes (red) and (b) CPA (blue) modes, where the solid and dashed curves are the corresponding even modes and odd modes, respectively. Also shown are the simulated electric-field patterns for (c) a laser mode and (d) a CPA mode (for $n' = 1.5$). In all the cases, $n' \geqslant 1$, $d = 2\lambda$, and $\lambda = 1$.

for CPA modes in a PIM slab could be treated as the case of a single incoming wave for perfect absorber (PA) modes in the semi-infinite spaces consisting of air and PIMs [see the schematic in Fig. 1(d), which is a simplification of the black dashed framed region in Fig. 1(c)]. The dispersion relationship for PA modes in the semi-infinite spaces is calculated as (for details, see Appendix A)

$$\frac{k_x\mu'}{k_x'} = 1, \tag{5}$$

where $k_x = \sqrt{k_0^2 - \beta^2}$, $k_x' = i\sqrt{\beta^2 - n'^2k_0^2}$, and $n'^2 = \varepsilon'\mu' = \varepsilon\mu$. From these equations, i.e., Eqs. (1)–(5) we find that $n' = 1$ is a special value, as $k_x = k_x'$ and the effective refractive index of PIMs is 1 and thus equal to that in the air background medium. Therefore, in the following we will explore the case of a PIM slab with $n' \geqslant 1$ in air and then investigate the case of a PIM slab with $0 < n' < 1$ in air. For simplicity, $\varepsilon = \mu = n'$ is set for PIMs to demonstrate the underlying physical behaviors.

A. Purely imaginary metamaterials with $n' \geqslant 1$

In this section we will investigate the PIM slab with $n' \geqslant 1$. Based on Eqs. (1)–(4), the corresponding dispersion relationships between the effective refractive index n' of the PIM slab and the propagation constant β are displayed in Figs. 2(a) and 2(b), which are the cases of laser modes (red) and CPA modes (blue), respectively. The solid and dashed curves are the corresponding even modes and odd modes. For $n' = 1.5$ as an example [see Figs. 2(a) and 2(b)], we choose the propagation constants $\beta = 0.627k_0$ and $\beta = 0.577k_0$ to obtain the laser mode and CPA mode, respectively. To verify the analytical results, we carry out numerical simulations by using a COMSOL Multiphysics–based finite-element method. For instance, to match the tangential momentum of the laser mode, i.e.,$\beta = 0.627k_0$, the wave with incident angle $\theta = 38.80^\circ$ strikes from the left side on the PIM slab [see the white arrow in Fig. 2(c)] and then the incoming wave oscillates inside the slab to accumulate energy, similar to the mechanism of laser

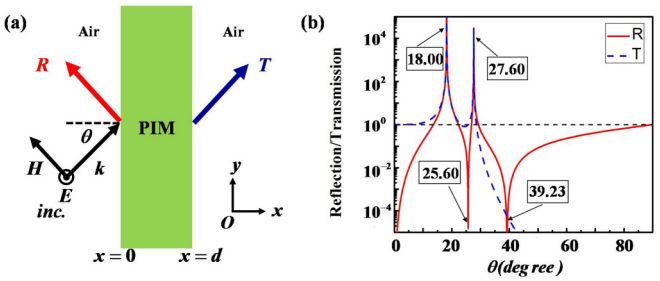

FIG. 3. (a) Schematic diagram of a PIM slab placed in air. (b) Relationships between transmission and reflection of the PIM slab and the incident angle on a logarithmic scale. The working wavelength is $\lambda = 1$ and the thickness of slab is $d = 2\lambda$. For the slab, we set $\varepsilon' = -0.5i$ and $\mu' = 0.5i$.

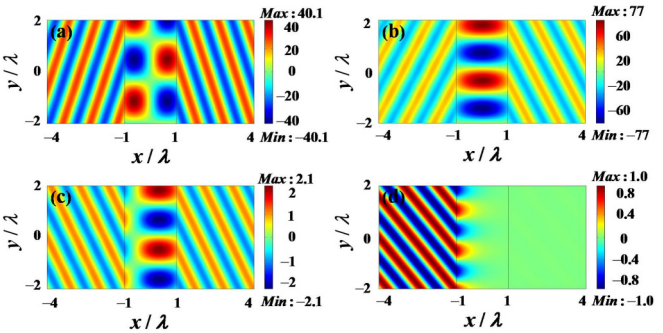

FIG. 4. Simulated electric-field patterns for the TE plane-wave incident on the PIM slab with different incident angles: (a) $\theta = 18.00^\circ$, (b) $\theta = 27.60^\circ$, (c) $\theta = 25.60^\circ$, and (d) $\theta = 39.23^\circ$.

modes in the cavity systems with gain media. As a result, the amplified electric field emits in the $-x$ and $+x$ directions by observing the field pattern and energy flux (black arrows) in Fig. 2(c), in which quite intense reflection and transmission take place on the left and right sides of the PIM slab.

To excite a CPA mode, the two incoming waves must be coherent with a specific amplitude and phase relationship at the boundaries (for details, see Appendix A). With A and D as the complex amplitudes of the two incoming coherent waves, a CPA requires either $A = D$ (symmetric mode) or $A = -D$ (antisymmetric mode). When the in-phase coherent waves ($A = D$) with $\theta = \pm 35.20^\circ$ are incident from the left and right sides [see the pair of white arrows in Fig. 2(d)], they match one of the tangential wave numbers of the CPA modes, i.e., $\beta = 0.577k_0$. As such, a CPA is produced by the combination of destructive interference and dissipation in the PIM slab, which is demonstrated well by observing the field pattern and energy fluxes (black arrows) in Fig. 2(d). Therefore, both laser modes and CPA modes are supported in a PIM slab, if the tangential momenta are matched.

B. Purely imaginary metamaterials with $0 < n' < 1$

As we know, total internal reflection should occur when light is incident from a medium with a higher refractive index to a medium with a lower one. It turns out that the physics is substantially different for PIMs with lower refractive indices. We consider a PIM slab with $0 < n' < 1$ placed in air schematically shown in Fig. 3(a). In the following we set $\varepsilon = \mu = n' = 0.5$ for the PIM slab as an example to reveal the underlying physics. Based on the general coefficients of transmission and reflection of a PIM slab [see Eqs. (B5) and (B6)], the corresponding relationships between transmission and reflection of the PIM slab and the incident angle are shown on a logarithmic scale in Fig. 3(b), where the red curve is the reflection ($R = |r|^2$) and the blue dashed curve is the transmission ($T = |t|^2$). From Fig. 3(b), we find that when the incident angle is near $\theta = 18.00^\circ$ or 27.60°, the transmission and reflection are extremely large. Moreover, when the incident angle is near $\theta = 25.60^\circ$ or 39.23°, the reflection is zero. In particular, for the incident angle with $\theta = 25.60^\circ$, the transmission is unity, which means that total transmission occurs. However, for the incident angle with $\theta = 39.23^\circ$, the transmission is almost zero, implying that no transmission and no reflection occur.

To verify the above intriguing results, numerical simulations are performed by using COMSOL Multiphysics. For example, when the wave with an incident angle of $\theta = 18.00^\circ$ impinges on the slab, the corresponding field pattern is shown in Fig. 4(a), with strong transmission and reflection. Likewise, for the wave with an incident angle of $\theta = 27.60^\circ$, the predicted strong transmission and reflection are seen in the field pattern in Fig. 4(b). The simulated field pattern for the incident wave with $\theta = 25.60^\circ$ is shown in Fig. 4(c), where the incident wave passes through the slab without any reflection and with unity transmission. For the incident wave with $\theta = 39.23^\circ$, which is beyond the critical angle $\theta_c = \arcsin n' = 30^\circ$, the corresponding field pattern is shown in Fig. 4(d) and it seems that the incident wave is bounded at the interface between air and PIM just like a surface wave, without any reflection and transmission.

To explain the above intense and vanishing transmission and reflection, we employ Eqs. (1)–(5) to display the corresponding dispersion relationships (n' vs β) for laser modes (red) and CPA (blue) modes in Figs. 5(a) and 5(b), where the solid curve and dashed curve are the corresponding even modes and odd modes, respectively, and the green dash-dotted curve is related to PA modes. For the case of $n' = 0.5$ shown in Figs. 5(a) and 5(b), the corresponding tangential propagation constants marked by the black dashed lines are $0.31k_0$, $0.46k_0$, and $0.63k_0$, which are consistent with the incident angles $\theta = 18.00^\circ$, 27.60°, and 39.23°, respectively. Therefore, the unusual transmission and reflection in Figs. 4(a), 4(b), and 4(d) are related to the excited laser modes and CPA mode, respectively. In fact, from Figs. 5(a) and 5(b), laser and CPA modes can be excited in the PIM slab with $0 < n' < 1$, if the incident angle θ is less than θ_c. However, for θ larger than θ_c, the transmission will be tremendously reduced, as total internal reflection happens [see, e.g., the transmission curve in Fig. 3(b)]. As a result, the laser modes do not exist for $\theta > \theta_c$, as wave decay will take place in the PIM slab.

However, CPA modes do exist in the case of $\theta > \theta_c$. For example, when the two incoming waves are incident on the slab, they will be bounded at the left and right interfaces without any reflection. For PIMs possessing higher refractive indices, the bounded waves inside the slab with a fixed thickness (here $d = 2\lambda$) do not interact with each other as their

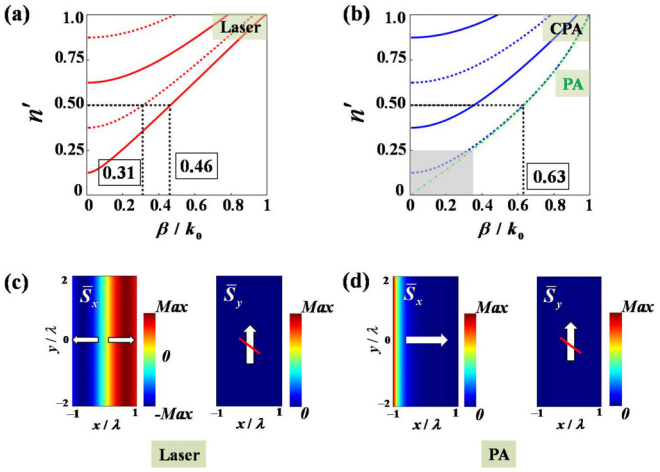

FIG. 5. Corresponding dispersion relationships (n' vs β) for (a) laser modes (red) and (b) CPA (blue) modes, where the solid and dashed curves are the corresponding even modes and odd modes, respectively. In (b) the green dash-dotted curve is related to the PA modes in the semi-infinite spaces. In all the cases, $0 < n' < 1$, $d = 2\lambda$, and $\lambda = 1$. Also shown are the simulated time-averaged energy fluxes in the x and y directions inside the PIM slab for the cases of (c) a laser mode and (d) a PA mode.

decay lengths are short. As a result [see Figs. 1(c) and 1(d)], the problem of two coherent incoming waves for CPA modes in a PIM slab will be treated as the case of a single incoming wave for PA modes in the semi-infinite spaces consisting of air and PIMs. Consequently, PA modes, which can perfectly absorb incident wave, could be realized in the PIM slab by replacing the coherent waves with a single incoming wave, which has been demonstrated in Fig. 4(d). This phenomenon is shown clearly in the dispersion relationships in Fig. 5(b), where the lowest blue dashed curve of CPA modes in the case of $\theta > \theta_c$ is coincident with the green dash-dotted curve of PA modes in the region of $n' > 0.25$, implying that CPA modes can be replaced by PA modes.

For $n' < 0.25$, marked in the gray region in Fig. 5(b), PA modes gradually deviate from CPA modes. In such a case, CPA modes can be realized in the PIM slab by the incoming coherent waves. For the single incident wave shining on the PIM slab, although there is no reflection, the transmitted wave will increase for the lower refractive indices of PIMs. Therefore, PA modes are not obtained in the PIM slab in this parameter regime. This is because for PIM slab with the lower refractive indices, the bound waves, which are from the two incoming coherent waves for realizing the CPA mode, interact with each other inside due to longer decayed lengths.

Furthermore, to clarify the behavior of the bounded wave inside the PIM slab, we analyze the time-averaged energy fluxes in the x and y directions inside the PIM slab, i.e., $\bar{S}_x = -\mathrm{Re}[H_y E_z^*]/2$ and $\bar{S}_y = \mathrm{Re}[H_x E_z^*]/2$, which can effectively reveal the energy flux distribution inside the slab. From the fields inside the PIM slab (for details, see Appendix C), we find $\bar{S}_y = 0$ in the PIM slab. In particular, $\bar{S}_x = k_x' \xi^2 \sin(k_x' x + \varphi)/\omega\mu_0\mu$ is a sinusoidal distribution inside the PIM slab for $\theta < \theta_c$ and $\bar{S}_x = \delta a_p^2 e^{-2\delta x}/2\omega\mu_0\mu$ is a decayed distribution for $\theta > \theta_c$. We also display the simulated time-averaged energy fluxes shown in Figs. 5(c) and 5(d), where the incident angles are $\theta = 27.60^\circ < \theta_c$ and $\theta = 39.23^\circ > \theta_c$ for the laser mode and PA mode, respectively. From the information in Figs. 5(c) and 5(d), inside the PIM slab, $\bar{S}_x$ exhibits the expected sinusoidal distribution for the excited laser mode and the decayed distribution for the PA mode, but $\bar{S}_y = 0$ in the PIM slab for both cases. The numerical results are thus consistent with the analytical results. Therefore, the bounded wave at the interface of the PIM slab and air in Fig. 4(d) is absorbed, rather than a surface wave propagating in the y direction. Furthermore, total transmission in Fig. 4(c) results from the Fabry-Pérot resonances, i.e., $\phi = k_x' d = m\pi$.

III. CONDITION FOR REALIZING CPA AND LASER MODES SIMULTANEOUSLY

By observing these dispersion relationships of $n' \geqslant 1$ [Figs. 2(a) and 2(b)] and $0 < n' < 1$ [see Figs. 5(a) and 5(b)], generally, CPA modes and laser modes take place in different conditions. In other word, for a fixed refractive index of the PIM slab, CPA modes and laser modes share different propagation constants β, which have been demonstrated for the cases of $n' = 1.5$ and $n' = 0.5$. However, in some cases where CPA and laser modes share opposite symmetric modes, CPA modes and laser modes could be realized simultaneously. To be exact, the odd laser modes [see Eq. (1)] can have a solution identical to the even CPA modes [see Eq. (4)], or the even laser modes [see Eq. (2)] can have the same solution as the odd CPA modes [see Eq. (3)]. In both cases, we can get a condition for realizing CPA modes and laser modes simultaneously with opposite symmetric modes, i.e., $\eta = k_x \mu'/k_x' = i$ with $\tan(k_x' d/2) = \pm 1$. After some simplification, such a condition for $d = 2\lambda$ can be further given as $\beta = 0$ with $n' = m/2 \pm 1/8 > 0$ ($m = 0,1,2,\ldots$) or $n' = 1$ with $\beta = 0.485k_0, 0.782k_0, 0.927k_0, 0.993k_0$. For $\beta = 0$, i.e., in the case of normal incidence [23,24], the required effective index of the PIM is $n' = 1/8,\ 3/8,\ 5/8,\ \ldots,(2m-1)/8$, which can clearly be found in Figs. 2(a), 2(b), 5(a), and 5(b), where CPA modes and laser modes happen simultaneously yet with opposite symmetric modes (see the curve styles of the dispersion curves). In addition, for $n' = 1$, there are some particular transverse propagation constants to realize CPA modes and laser modes simultaneously.

IV. CONCLUSION

We have analyzed the interaction of incident plane waves with uniform PIM slabs. We have found, both analytically and numerically, that CPA modes and laser modes are supported in the PIM slab and it is a mechanism different from that which occurs in PT-symmetric systems, in which loss and gain are separated in different regions. In addition, the general conditions for realizing CPA and laser modes have been derived. We also identify the conditions for realizing the CPA mode and laser mode simultaneously, with the case of normal incidence [22–24] as a special case. More interestingly, as a simplification of CPA modes, single-sided PA modes can be obtained in a PIM slab with a subunity effective index for the incident angle beyond the critical angle. Overall, we find that PIMs produce yet more unusual wave behavior that

can be realized through metamaterials. Although the equal amplitudes of EM parameters $\varepsilon = \mu$ are considered for PIMs to demonstrate these significant wave phenomena, similar phenomena can be realized in PIMs with $\varepsilon \neq \mu$ [because Eqs. (1)–(5) are satisfied with real solutions as well]. We acknowledge that PIMs are very hard to realize in practice as loss and gain parameters are included in the same medium. However, recently two schemes [23,24] to realize materials with properties similar to PIMs have been proposed. By employing PT-symmetric materials in layered structures [23], PIMs can be effectively mimicked, with the similar CPA-laser effect realized. The other method is that, based on the effective-medium theory [25], PIMs could be well designed by using a photonic crystal composed of core-shell rods [24], in which loss and gain media are distributed in either the cores or the shells. Therefore, considering the recent experimental progress in optical gain [17], PIMs might be realized experimentally in the future.

If we consider TM polarization in our proposed PIMs, similar wave phenomena can be still achieved. In particular, for PIMs with $\varepsilon = \mu$, the left-hand sides of Eqs. (1)–(4) will change the signs as $\eta_{\mathrm{TM}} = k_x\varepsilon'/k'_x = -k_x\mu'/k'_x = -\eta$. As a result, the dispersion relationships of laser (CPA) modes for TE polarization will be transformed into these of CPA (laser) modes for TM polarization. To be exact, for such a PIM slab of interest, when it is used to realize a laser (CPA) for TE polarization, accordingly, a CPA (laser) will be achieved for TM polarization. Therefore, our proposed PIMs can be employed to realize CPA and laser modes without the limit of polarizations, which are available for obtaining CPA and laser modes simultaneously. As CPA and laser modes can be effectively realized in our PIMs, PIMs also can be used to achieve negative refraction [26] and planar imaging [27], in which the CPA (as the time-reversed laser [28]) and laser are respectively obtained in the loss and gain media in PT-symmetric systems.

ACKNOWLEDGMENTS

This work was supported by the National Natural Science Foundation of China (Grant No. 11604229), the National Science Foundation of China for Excellent Young Scientists (Grant No. 61322504), the Postdoctoral Science Foundation of China (Grant No. 2015M580456), and the Fundamental Research Funds for the Central Universities (Grant No. 20720170015). We thank Professor Hong Chen for helpful discussions.

APPENDIX A: THE CPA AND LASER MODES OF A PIM SLAB

1. Laser modes

The general wave scatter0ing of a PIM slab ($\varepsilon' = -i\varepsilon$ and $\mu' = i\mu$, ε and μ are positive real numbers) includes incoming waves (blue dashed arrows) and outgoing waves (red solid arrows) and is schematically shown in Fig. 1(a). For laser modes, the injected signals (incoming waves) can be ignored, as the outgoing waves are extremely powerful compared with the incoming waves, and the schematic of wave scattering is plotted in Fig. 1(b). Therefore, the corresponding electric-field distributions in different regions can be written as

$$\vec{E}_1 = Ae^{-ik_x x}e^{i\beta y}\hat{z}, \quad x < 0 \tag{A1}$$

$$\vec{E}_2 = (Be^{ik'_x x} + Ce^{-ik'_x x})e^{i\beta y}\hat{z}, \quad 0 < x < d \tag{A2}$$

$$\vec{E}_3 = De^{ik_x(x-d)}e^{i\beta y}\hat{z}, \quad x > d \tag{A3}$$

and the corresponding magnetic-field distributions can be obtained by the Maxwell equation $\vec{H} = \vec{\nabla} \times \vec{E}/i\omega\mu_0\mu$. By matching the boundary conditions at the interfaces $x = 0$ and $x = d$, the dispersion relationships for laser modes are

$$\eta = -i\cot\left(k'_x\frac{d}{2}\right) \quad \text{(odd modes)}, \tag{A4}$$

$$\eta = i\tan\left(k'_x\frac{d}{2}\right) \quad \text{(even modes)}, \tag{A5}$$

where $\eta = k_x\mu'/k'_x$, $k_x = \sqrt{k_0^2 - \beta^2}$, $k'_x = \sqrt{n'^2k_0^2 - \beta^2}$, and $n'^2 = \varepsilon'\mu'$. Consider that the excited wave is plane-wave incident from air with $\beta \leqslant k_0$ and then $k_x = \sqrt{k_0^2 - \beta^2} > 0$.

If the slab is composed of PIMs ($\varepsilon = \mu$ or $\varepsilon \neq \mu$), ε' and μ' are purely imaginary numbers.

(a) For $\beta \leqslant n'k_0$, $\eta = k_x\mu'/k'_x$ is purely imaginary number and the right-hand sides of Eqs. (A4) and (A5) are also purely imaginary numbers.

(b) For $\beta > n'k_0$, $\eta = k_x\mu'/k'_x$ is a real number. As $k'_x = i\sqrt{n'^2k_0^2 - \beta^2}$ is purely imaginary number, the right-hand sides of Eqs. (A4) and (A5) are real numbers.

Therefore, Eqs. (A4) and (A5) can be satisfied with real solutions for β. As a wave from air possesses a real tangential wave vector, perfect excitation for laser modes will happen owing to momentum matching. As a result, PIMs can support perfect laser modes.

However, if the slab is made of CMs with real parts, i.e., $\alpha \neq \pi/2$, ε' and μ' are complex numbers.

(c) For $\beta \leqslant n'k_0$, $\eta = k_x\mu'/k'_x$ is complex number, while the right-hand sides of Eqs. (A4) and (A5) are purely imaginary numbers.

(d) For $\beta > n'k_0$, $\eta = k_x\mu'/k'_x$ is a complex number; as $k'_x = i\sqrt{n'^2k_0^2 - \beta^2}$ is imaginary number, the right-hand sides of Eqs. (A4) and (A5) are real numbers.

Therefore, Eqs. (A4) and (A5) are not satisfied with real solutions for β. As a wave from air possesses a real tangential wave vector, perfect excitation for laser modes will not happen due to momentum mismatching. As a result, the performance of the laser modes will decrease and CMs with $\alpha \neq \pi/2$ do not support perfect laser modes.

2. Coherent perfect absorber modes

To obtain CPA modes, the outgoing signals can be ignored, i.e., the outgoing waves are zero; the schematic of wave scattering is plotted in Fig. 1(c). Therefore, the corresponding

electric-field distributions in different regions can be written as

$$\vec{E}_1 = Ae^{ik_x x}e^{i\beta y}\hat{z}, \quad x < 0 \tag{A6}$$

$$\vec{E}_2 = (Be^{ik'_x x} + Ce^{-ik'_x x})e^{i\beta y}\hat{z}, \quad 0 < x < d \tag{A7}$$

$$\vec{E}_3 = De^{-ik_x(x-d)}e^{i\beta y}\hat{z}, \quad x > d \tag{A8}$$

and the corresponding magnetic-field distributions can be figured out by the Maxwell equation $\vec{H} = \vec{\nabla} \times \vec{E}/i\omega\mu_0\mu$. By matching the boundary conditions at the interfaces $x = 0$ and $x = d$, the dispersion relationships for CPA modes are

$$\eta = i \cot\left(k'_x \frac{d}{2}\right) \quad \text{(odd modes)}, \tag{A9}$$

$$\eta = -i \tan\left(k'_x \frac{d}{2}\right) \quad \text{(even modes)}, \tag{A10}$$

where $\eta = k_x\mu'/k'_x$, $k_x = \sqrt{k_0^2 - \beta^2}$, $k'_x = \sqrt{n'^2 k_0^2 - \beta^2}$, and $n'^2 = \varepsilon'\mu'$.

Similar to the discussion of laser modes, perfect excitation of CPA modes can only exist in PIMs ($\varepsilon = \mu$ or $\varepsilon \neq \mu$). For realizing CPA modes, the two incident signals should be coherent with a specific amplitude and phase relationship at the boundaries, i.e., $A = (1 - \eta)/(1 + \eta)e^{-ik'_x d}D$.

3. Perfect absorber modes

In our PIM slab with the effective refractive index less than 1, when the incident angle θ is beyond θ_c, the incident wave could be perfectly bounded at the interface between air and PIM without any reflection and transmission, defined as perfect absorber modes. When the two incoming waves for a CPA are incident on the slab, they will be bounded at the left and right interfaces. For a PIM slab with a fixed thickness, when PIMs possess a higher effective refractive index, it is difficult for the bounded waves inside the slab to interact with each other, which can effectively throttle the outgoing waves. In this situation, the problem of CPA modes will become the case of PA modes in the semi-infinite spaces consisting of air and PIMs as shown in Fig. 1(d). For this case, the electric-field distributions in air ($x < 0$) and PIM media ($x \geqslant 0$) can be respectively written as

$$\vec{E}_1 = Ae^{ik_x x}e^{i\beta y}\hat{z}, \quad x < 0 \tag{A11}$$

$$\vec{E}_2 = Be^{-ik'_x x}e^{i\beta y}\hat{z}, \quad x \geqslant 0 \tag{A12}$$

and the corresponding magnetic-field distributions can be obtained by the Maxwell equation $\vec{H} = \vec{\nabla} \times \vec{E}/i\omega\mu_0\mu$. By matching the boundary conditions at the interface $x = 0$, the dispersion relationship for PA modes is

$$\frac{k_x\mu'}{k'_x} = 1, \tag{A13}$$

where $k_x = \sqrt{k_0^2 - \beta^2}$, $k'_x = i\sqrt{\beta^2 - n'^2 k_0^2}$, and $n'^2 = \varepsilon'\mu'$.

If the slab is composed of PIMs ($\varepsilon = \mu$ or $\varepsilon \neq \mu$), ε' and μ' are purely imaginary numbers, then Eq. (A13) can be satisfied with real solutions for β. In contrast, for CMs with real parts, there are complex solutions for β. Hence, for our proposed PIMs, PA modes can exist.

APPENDIX B: TRANSMISSION AND REFLECTION OF A PIM SLAB IN AIR

Now we consider the reflection and refraction for a PIM slab in air [see Fig. 3(a)]. Suppose the two interfaces of the CM slab and air are $x = 0$ and $x = d$, where d is the thickness of the slab. For an incident plane wave

$$\vec{E}_{\text{int}} = e^{ik_x x + i\beta y}\hat{z}, \quad x < 0 \tag{B1}$$

the reflected wave is written as

$$\vec{E}_{\text{ref}} = re^{-ik_x x + i\beta y}\hat{z}, \quad x < 0, \tag{B2}$$

while the transmitted wave is expressed as

$$\vec{E}_{\text{trn}} = te^{ik_x(x-d) + i\beta y}\hat{z}, \quad x > d, \tag{B3}$$

where $\beta = k_0 \sin\theta$ is the wave vector along the slab, $k_x = k_0 \cos\theta$ and $k'_x = k_0\sqrt{\varepsilon'\mu' - \sin^2\theta}$ are the wave vectors normal to the slab in air and CM slab, respectively, θ is the incident angle, and r and t are the coefficients of reflection and transmission, respectively.

For the PIM slab,

$$\vec{E}_{\text{PIM}} = (a_p e^{ik'_x x + i\beta y} + a_n e^{-ik'_x x + i\beta y})\hat{z}, \quad 0 \leqslant x \leqslant d, \tag{B4}$$

where a_p and a_n are the corresponding coefficients of positive and negative components. After matching the boundary conditions at the interfaces of $x = 0$ and $x = d$, we have

$$r = \frac{(1 - \eta^2)2i \sin\phi}{(1 + \eta)^2 \exp(-i\phi) - (1 - \eta)^2 \exp(i\phi)}, \tag{B5}$$

$$t = \frac{4\eta}{(1 + \eta)^2 \exp(-i\phi) - (1 - \eta)^2 \exp(i\phi)}, \tag{B6}$$

$$a_p = \frac{2(\eta^2 + \eta)}{(1 + \eta)^2 - (1 - \eta)^2 \exp(2i\phi)}, \tag{B7}$$

$$a_n = \frac{2(\eta - \eta^2)\exp(2i\phi)}{(1 + \eta)^2 - (1 - \eta)^2 \exp(2i\phi)}, \tag{B8}$$

where $\eta = k_x\mu'/k'_x$ and $\phi = k'_x d$ is the phase change in the slab.

APPENDIX C: ENERGY FLUX IN A PIM SLAB

Based on the results in Appendix B, the corresponding EM wave inside the PIM slab can be written as

$$\vec{E}_z = (a_p e^{ik'_x x} + a_n e^{-ik'_x x})e^{i\beta y}\hat{z}, \tag{C1}$$

$$\vec{H}_x = \frac{\beta}{\omega\mu_0\mu'}(a_p e^{ik'_x x} + a_n e^{-ik'_x x})e^{i\beta y}\hat{x}, \quad \text{(C2)}$$

$$\vec{H}_y = -\frac{k'_x}{\omega\mu_0\mu'}(a_p e^{ik'_x x} - a_n e^{-ik'_x x})e^{i\beta y}\hat{y}. \quad \text{(C3)}$$

The time-averaged energy fluxes in the x and y directions are given as $\bar{S}_x = -\mathrm{Re}(H_y E_z^*)/2$ and $\bar{S}_y = \mathrm{Re}(H_x E_z^*)/2$.

(a) For the EM wave in the PIM slab wave being propagating wave ($\sqrt{\varepsilon'\mu'} \geqslant \sin\theta$), $\beta = k_0 \sin\theta$ and $k'_x = k_0\sqrt{\varepsilon'\mu' - \sin^2\theta}$. As $\eta = k_x\mu'/k'_x$ is a purely imaginary number, based on Eqs. (B7) and (B8), we can easily deduce $a_p = a_n^*$ and $\vec{E}_z^{\,*} = (a_p^* e^{-ik'_x x} + a_n^* e^{ik'_x x})e^{-i\beta y}\hat{z}$; therefore,

$$\bar{S}_x = -\frac{1}{2}\mathrm{Re}[H_y E_z^*] = -\frac{1}{2}\mathrm{Re}\left[-\frac{k'_x}{\omega\mu_0\mu'}\left(a_p^2 e^{2ik'_x x} - a_n^2 e^{-2ik'_x x}\right)\right],$$

$$\bar{S}_y = \frac{1}{2}\mathrm{Re}[\mathrm{H_x E_z^*}] = \frac{1}{2}\mathrm{Re}\left[\frac{\beta}{\omega\mu_0\mu'}\left(|a_p|^2 + |a_n|^2 + a_p^2 e^{2ik'_x x} + a_n^2 e^{-2ik'_x x}\right)\right].$$

We assume $a_p = \xi e^{i\varphi}$ and $a_n = \xi e^{-i\varphi}$; then

$$\bar{S}_x = -\frac{1}{2}\mathrm{Re}\left[-\frac{k'_x}{\omega\mu_0\mu'}(2i\xi^2 \sin(k'_x x + \varphi))\right] = \frac{k'_x}{\omega\mu_0\mu}\xi^2 \sin(k'_x x + \varphi) \quad \text{(C4)}$$

$$\bar{S}_y = -\frac{1}{2}\mathrm{Re}\left[\frac{i\beta}{\omega\mu_0\mu}\{2\xi^2[\cos(k'_x x + \varphi) + 1]\}\right] = 0. \quad \text{(C5)}$$

(b) For the EM waves in the PIM slab being decayed waves ($\sqrt{\varepsilon'\mu'} < \sin\theta$), $\beta = k_0 \sin\theta$ and $k'_x = ik_0\sqrt{\sin^2\theta - \varepsilon'\mu'} = i\delta$. As $\exp(2i\phi) = \exp(-2\delta d) \to 0$, we have $a_p = 2\eta/(1+\eta)$, with $\eta = k_x\mu'/k'_x = k_x\mu/\delta$, $k_x = k_0\cos\theta$, and $a_n = 0$. As a result, as $\eta = k_x\mu'/k'_x = k_x\mu/\delta$ is a real number and a_p is also a real one, we have

$$\bar{S}_x = -\frac{1}{2}\mathrm{Re}\left[-\frac{i\delta}{\omega\mu_0\mu'}a_p^2 e^{-2\delta x}\right] = \frac{\delta}{2\omega\mu_0\mu}a_p^2 e^{-2\delta x}, \quad \text{(C6)}$$

$$\bar{S}_y = \frac{1}{2}\mathrm{Re}\left[\frac{-i\beta}{\omega\mu_0\mu}a_p^2 e^{-2\delta x}\right] = 0. \quad \text{(C7)}$$

Therefore, based on the above results, we can conclude that the energy flux in the PIM slab only propagates in the x direction as $\bar{S}_y = 0$ always happens in the PIM slab.

[1] W. Cai and V. M. Shalaev, *Optical Metamaterials: Fundamentals and Applications* (Springer, Berlin, 2009).
[2] Y. Xu, Y. Fu, and H. Chen, Nat. Rev. Mater. **1**, 16067 (2016).
[3] D. Schurig, J. J. Mock, B. J. Justice, S. A. Cummer, J. B. Pendry, A. F. Starr, and D. R. Smith, Science **314**, 977 (2006).
[4] T. Ergin, N. Stenger, P. Brenner, J. B. Pendry, and M. Wegener, Science **328**, 337 (2010).
[5] J. B. Pendry, Phys. Rev. Lett. **85**, 3966 (2000).
[6] R. A. Shelby, D. R. Smith, and S. Schultz, Science **292**, 77 (2001).
[7] H. Chen and C. T. Chan, Appl. Phys. Lett. **90**, 241105 (2007).
[8] H. Chen, B. Hou, S. Chen, X. Ao, W. Wen, and C. T. Chan, Phys. Rev. Lett. **102**, 183903 (2009).
[9] Y. Lai, J. Ng, H. Chen, D. Han, J. Xiao, Z. Zhang, and C. T. Chan, Phys. Rev. Lett. **102**, 253902 (2009).
[10] Y. Xu, S. Du, Lei Gao, and H. Chen, New J. Phys. **13**, 023010 (2011).
[11] Z. Lin, H. Ramezani, T. Eichelkraut, T. Kottos, H. Cao, and D. N. Christodoulides, Phys. Rev. Lett. **106**, 213901 (2011).
[12] Y. Fu, Y. Xu, and H. Y. Chen, Opt. Express **24**, 1648 (2016).
[13] S. Longhi, Phys. Rev. A **82**, 031801 (2010).
[14] Y. D. Chong, L. Ge, and A. D. Stone, Phys. Rev. Lett. **106**, 093902 (2011).
[15] Y. Sun, W. Tan, H. Q. Li, J. Li, and H. Chen, Phys. Rev. Lett. **112**, 143903 (2014).
[16] H. Hodaei, M. A. Miri, M. Heinrich, D. N. Christodoulides, and M. Khajavikhan, Science **346**, 975 (2014).
[17] Z. Wong, Y. Xu, J. Kim, K. OBrien, Y. Wang, L. Feng, and X. Zhang, Nat. Photon. **10**, 796 (2016).
[18] H. Ramezani, D. N. Christodoulides, V. Kovanis, I. Vitebskiy, and T. Kottos, Phys. Rev. Lett. **109**, 033902 (2012).
[19] N. Lazarides and G. P. Tsironis, Phys. Rev. Lett. **110**, 053901 (2013).
[20] Y. D. Xu, Y. Y. Fu, and H. Y. Chen, Opt. Express **25**, 4952 (2017).
[21] D. Dragoman, Opt. Commun. **284**, 2095 (2011).
[22] A. Basiri, I. Vitebskiy, and T. Kottos, Phys. Rev. A **91**, 063843 (2015).
[23] S. Xiao, J. Gear, S. Rotter, and J. Li, New J. Phys. **18**, 085004 (2016).
[24] P. Bai, K. Ding, G. Wang, J. Luo, Z. Zhang, C. T. Chan, Y. Wu, and Y. Lai, Phys. Rev. A **94**, 063841 (2016).
[25] Y. Wu, J. Li, Z. Q. Zhang, and C. T. Chan, Phys. Rev. B **74**, 085111 (2006).
[26] R. Fleury, D. L. Sounas, and A. Alù, Phys. Rev. Lett. **113**, 023903 (2014).
[27] F. Monticone, C. A. Valagiannopoulos, and A. Alù, Phys. Rev. X **6**, 041018 (2016).
[28] W. Wan, Y. Chong, L. Ge, H. Noh, A. D. Stone, and H. Cao, Science **331**, 889 (2011).